Journal of Engineering Mathematics **28**: 463–482, 1994.

Thermosolutal convection between poorly conducting plates

S.M. COX

Department of Applied Mathematics, The University of Adelaide, Adelaide 5005, Australia

Received 9 March 1993; accepted in revised form 18 December 1993

Key words: convection, long-wave asymptotics, hydrodynamic stability

Abstract. Thermosolutal convection is considered in a fluid layer between poorly conducting horizontal boundaries. The horizontal scale of the motions is much greater than the depth of the fluid layer, provided the motion is not too vigorous, and this disparity between horizontal and vertical scales provides the basis for an asymptotic expansion of the solution. Under the assumption of near-constant solute-flux at the horizontal boundaries, a pair of evolution equations is derived for the depth-averaged temperature and solute concentration fields.

These long-wave equations are investigated for two-dimensional convection by numerical integrations, and the results are compared with linear and weakly non-linear theory. The asymptotic expansion is shown to break down for large values of R, when the form assumed for the convection becomes inappropriate.

The onset of three-dimensional convection is analysed. Steady square convection cells are stable. Oscillatory convection in the form of two-dimensional travelling-wave rolls is stable to three-dimensional disturbances near onset.

1. Introduction

Doubly-diffusive convection has a wide range of applications across many scientific disciplines, including oceanography [1–3], astrophysics [4], metallurgy, geophysics [5, 6]. It arises as a generalization of thermal convection, when a second diffusing species is present.

The first studies of doubly-diffusive convection were in oceanography, where thermosolutal convection is driven by gradients in heat and salt concentration. A more recent application in oceanography is to Langmuir circulations, which are wind-driven counter-rotating vortices in the upper layer of oceans and lakes. A two-dimensional model due to Craik and Leibovich describes the circulations by equations which are mathematically identical to those for thermosolutal convection, but with temperature and salt concentration replaced by a wind-directed velocity and a temperature, respectively [7–11]. An important industrial application of doubly-diffusive convection concerns crystal growth from a melt. Hydrodynamic instabilities generate convection in the melt, with heat and melt composition as the diffusing species. The convective motions lead to variations in the crystal growth rate, or to irregularities in the crystal, and the interest is in eliminating or controlling the convection. Convection in large stars [4] is subject to many diffusing components (angular momentum, heat, the magnetic field, the composition), although the best-studied effects arise from the double diffusion of heat and magnetic flux. The equations governing such magnetoconvection are analogous to those for thermosolutal convection, as treated here. Flow in magma chambers is also a doubly-diffusive (or perhaps multiply-diffusive) system, as crystallization generates concentration gradients in the magma [5].

In this paper we investigate the non-linear dynamical behaviour of thermosolutal convection in a layer of fluid between horizontal plates, heated and salted from below. The boundary plates are assumed to be poor conductors of heat, in which case the first instability as the thermal Rayleigh number is increased is to rolls with a width much greater than the depth of the layer. The consequences of the large aspect-ratio of the motions have been discussed for mantle convection by Hewitt et al. [12], and for solar convection by Depassier and Spiegel [13]. The long-wave onset of Rayleigh–Bénard (that is, purely thermal) convection has been examined theoretically according to linearized theory [14–16], and a fully non-linear theory has been developed [17–19], in which a 'shallow-water' expansion of the solution yields as its first non-trivial solvability condition a non-linear evolution equation for the depth-averaged temperature field. This equation has a Lyapunov functional, and so its asymptotic solution at large times must be time-independent. The expansion does not assume that the disturbances are small. Other convective systems have been treated similarly (e.g., Marangoni convection by Sivashinsky [20]).

If a constant solute flux is maintained at the boundaries (rather than the usual condition of a constant solute concentration there) then *two* evolution equations emerge from a similar long-wave expansion of the thermosolutal problem, one equation for each of the depth-averaged temperature and solute concentration fields [21]. These equations permit both steady and oscillatory convection. A linear stability analysis and weakly non-linear treatment of the onset of two-dimensional convection has been carried out in [21]. A bifurcation picture is found which agrees qualitatively with that for 'ideal double diffusion' (between stress-free, isothermal, isosaline boundaries [2, 3]), and with that for Langmuir circulation [7].

We describe numerical simulations of the two-dimensional long-wave equations, for Prandtl and Lewis numbers appropriate to heat and salt in water (the oceanographic case), and for Langmuir circulation. We compare our results with the theoretical predictions, and find good agreement. We are able to compute steady rolls, travelling waves, and in very small regions of parameter space we have found modulated travelling waves (that is, travelling waves with a temporally modulated amplitude) and standing waves.

According to the long-wave expansion described here the convective motions are weak, even when the dimensionless temperature and solute fields are $O(1)$. Such an assumption is reasonable near the onset of instability, but does not hold when the thermal Rayleigh number is large, and the long-wave expansion breaks down. We discuss this break-down, and show how it manifests itself in our numerical simulations.

The two-dimensional thermosolutal convection problem is outlined in Section 2. The long-wave expansion, linear stability matters, and weakly non-linear results are sketched in Section 3, and are compared with ideal double diffusion in Section 4. Numerical simulations of the long-wave equations follow in Section 5, and a discussion of the breakdown of the expansion comprises Section 6. In Section 7 we analyse the steady and Hopf bifurcations in three-dimensional convection, in a square periodic geometry. In three dimensions the analogy between thermosolutal convection and Langmuir circulation is lost. Proctor [19] and Knobloch [22] have examined the stability of the long-wave two-dimensional steady rolls to cross-roll perturbations, and find squares to be the preferred planform of steady three-dimensional Boussinesq Rayleigh–Bénard convection when symmetrical boundary conditions apply at upper and lower boundaries. We extend their work, and in particular we treat the Hopf bifurcation. Our conclusions are presented in Section 8.

2. Problem description

Two-dimensional thermosolutal convection between horizontal planes may be described by the following equations for the dimensionless flow quantities:

$$\begin{aligned}
&\frac{1}{\sigma}\left(\frac{\partial \nabla^2\psi}{\partial t} - J(\psi, \nabla^2\psi)\right) = R\frac{\partial\theta}{\partial y} - S\frac{\partial\Sigma}{\partial y} + \nabla^4\psi \\
&\left(\frac{\partial}{\partial t} - \nabla^2\right)\theta = \frac{\partial\psi}{\partial y} + J(\psi, \theta) \\
&\left(\frac{\partial}{\partial t} - \tau\nabla^2\right)\Sigma = \frac{\partial\psi}{\partial y} + J(\psi, \Sigma)\,,
\end{aligned} \tag{1}$$

where $J(a, b) \equiv a_y b_z - a_z b_y$ (the Jacobian) is the non-linear advection term. Here y and z are, respectively, the horizontal and vertical coordinates, and ψ is the streamfunction; the y- and z-velocity components are $v = \psi_z$ and $w = -\psi_y$, respectively. The temperature field is $T = T_0 - z + \theta(y, z, t)$, where $T_0 - z$ is the linear conduction solution, and θ the perturbation. Similarly, the solute concentration field is $C = C_0 - z + \Sigma(y, z, t)$. The parameters R and S are, respectively, thermal and solutal Rayleigh numbers; τ and σ are Lewis and Prandtl numbers, respectively [2, 3, 23]. Throughout this paper we shall assume $\tau < 1$ (this is true in particular for the case of heat and salt in water, and for Langmuir circulation). We have non-dimensionalized the depth of the fluid so that the upper and lower planes bounding the flow are at $z = 0, -1$ $(= -1/2 \pm 1/2)$. The two-dimensional Laplacian is $\nabla^2 = \partial_y^2 + \partial_z^2$.

We shall consider in this paper convection between almost-insulating horizontal boundaries, so that θ satisfies

$$\partial\theta/\partial z \pm \alpha_\pm\theta = 0 \quad \text{on } z = -1/2 \pm 1/2\,, \tag{2}$$

where α_+ and α_- are small non-negative constants [19, 24]. If a constant flux of solute is maintained through the walls then $\partial\Sigma/\partial z = 0$ there. We shall allow a generalization of this boundary condition, similar to a 'Newton's law of cooling' [15]:

$$\partial\Sigma/\partial z \pm \gamma_\pm\Sigma = 0 \quad \text{on } z = -1/2 \pm 1/2\,,$$

with $\gamma_+, \gamma_- \geqslant 0$. In the context of Langmuir circulation, where the quantity Σ is in fact the temperature perturbation, the mixed boundary conditions on Σ have the same interpretation as (2); the boundary conditions on Σ also arise naturally in other applications (for example, Sivashinsky discusses its relevance to the solidification of a dilute binary alloy in [25]). In the long-wave equations derived below, the Biot numbers α_+, α_-, γ_+ and γ_- appear only in the combinations $\alpha \equiv \alpha_+ + \alpha_-$ and $\gamma \equiv \gamma_+ + \gamma_-$ (to the order to which we carry the expansion).

We shall consider two choices for the momentum boundary conditions: (i) no-slip boundaries at top and bottom ('rigid-rigid'), or (ii) stress-free boundaries ('free-free'). Other choices may be contemplated, but will not change the form of the long-wave equations provided that the same boundary conditions are applied to ψ at $z = 0$ and $z = -1$. If this up-down symmetry is broken new terms appear in the evolution equations to be derived, and this circumstance is beyond the scope of this paper. 'Rigid-rigid' boundaries require $\psi = \psi_z = 0$ on $z = 0, -1$; 'free-free' boundaries that $\psi = \psi_{zz} = 0$ on $z = 0, -1$.

Convective motion in the layer corresponds to non-trivial solutions of (1) for ψ. To

determine when convection is possible we examine the linear stability of the trivial solution to (1) by dropping the non-linear terms and calculating the growth rate s of eigenmodes proportional to $\exp\{iky + st\}$. This eigenvalue problem must in general be solved numerically (our method is described in [7, 8]). As R is increased through a threshold value $R_c(S, \tau, \sigma, \alpha_\pm, \gamma_\pm)$ the trivial solution of (1) becomes unstable when the largest real part of the eigenvalues becomes positive. The wavenumber of this critical eigenmode is denoted by k_c. When α is small in (2) the critical wavenumber k_c is also small; in fact $k_c = O(\alpha^{1/4})$ as $\alpha \to 0$ [18–22, 25–27]. When $\gamma \gg \alpha$ the bifurcation is always steady, that is, $s = 0$ at the onset of instability [26]. Alternatively, if $\gamma \leq O(\alpha)$, in particular if $\gamma = 0$, then the bifurcation may be either steady ($s = 0$) or oscillatory (a Hopf bifurcation: $s = \pm i\omega$ at onset). These steady and oscillatory bifurcations, and the consequent modes of convection are the subject of this paper.

3. The long-wave limit

Figures 1 and 2 illustrate marginal stability curves for (1) when $\alpha = 0$, and when $\alpha > 0$ is small, computed using the method described in [7, 8]. It is clear that, at least not too far above the onset of instability, small values of wavenumber k are significant, and motions are likely to occur on a horizontal scale much greater than the depth of the layer (which has been scaled to unity). Such an intuition based on the linear theory is confirmed by non-linear considerations [17, 19]. A consistent expansion of the solution to (1) under the assumption of slow horizontal spatial variations (made in detail in [26]) yields the following:

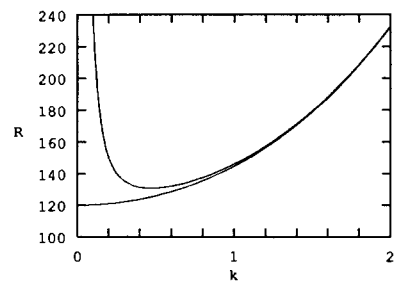

Fig. 1. Marginal stability curves for (1): critical thermal Rayleigh number is plotted against wavenumber k of the perturbation. The lower curve is for $\alpha = 0$, and is distinguished by the vanishing of the critical wavenumber ($k_c = 0$). The upper curve is for $\alpha_\pm = 0.005$, so that $\alpha = 0.01$: now $k_c > 0$, and the convection has a finite horizontal scale at onset. Other parameters: $S = 0$, $\sigma = 7$, $\tau = 1/80$, $\gamma = 0$ (and 'free-free' boundaries). The bifurcation is steady.

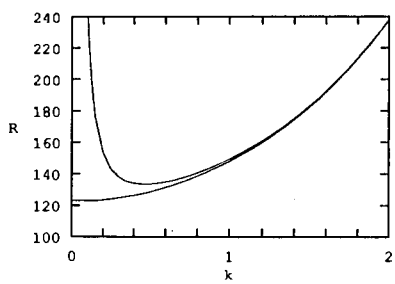

Fig. 2. Marginal stability curve for (1). Same as Fig. 1, except that $S = 1$ and the bifurcation is oscillatory.

$$\theta = \bar{\theta}(y,t) + \epsilon\theta_2(y,z,t) + O(\epsilon^2)$$
$$\Sigma = \bar{\Sigma}(y,t) + \epsilon\Sigma_2(y,z,t) + O(\epsilon^2) \tag{3}$$
$$\psi = \epsilon^{1/2}\psi_1(y,z,t) + O(\epsilon^{3/2}),$$

where $\bar{\theta}, \bar{\Sigma} = O(1)$, $\alpha, \gamma = O(\epsilon^2)$, and the horizontal length scale is $\epsilon^{-1/2}y$. Here ϵ^2 is intended to indicate the order of magnitude of the small parameter α. We may define ϵ unambiguously by choosing $\epsilon^2 = \alpha/\bar{\alpha}$, where $\bar{\alpha}$ is any constant of $O(1)$, for example we may set $\epsilon^2 = \alpha$. However, our results do not depend on the choice of $\bar{\alpha}$.

Vertical diffusion of temperature and solute dominates, and so θ and Σ are to leading order independent of depth. The streamfunction is, at leading order, $\psi_1 = (S\,\partial\bar{\Sigma}/\partial y - R\,\partial\bar{\theta}/\partial y)F(z)$, where $F(z) = z^2(1+z)^2/24$ for 'rigid-rigid' boundaries, and $F(z) = (z^4 + 2z^3 - z)/24$ for 'free-free' boundaries. (These expressions agree with [17] for Rayleigh–Bénard convection, when S is set to zero.)

At $O(\epsilon^2)$ in the expansion a solvability condition requires that the z-averages $\bar{\theta}$ and $\bar{\Sigma}$ satisfy the PDEs

$$\frac{\partial\bar{\theta}}{\partial t} = -\alpha\bar{\theta} + \frac{\partial^2}{\partial y^2}[\bar{\theta} + d(S\bar{\Sigma} - R\bar{\theta})] - a\frac{\partial^4\bar{\theta}}{\partial y^4} + b\frac{\partial^4\bar{\Sigma}}{\partial y^4} + \tau c\frac{\partial}{\partial y}\left[\frac{\partial\bar{\theta}}{\partial y}\left(R\frac{\partial\bar{\theta}}{\partial y} - S\frac{\partial\bar{\Sigma}}{\partial y}\right)^2\right],$$
$$\frac{\partial\bar{\Sigma}}{\partial t} = -\tau\gamma\bar{\Sigma} + \frac{\partial^2}{\partial y^2}[\tau\bar{\Sigma} + d(S\bar{\Sigma} - R\bar{\theta})] - a\frac{\partial^4\bar{\theta}}{\partial y^4} + b\frac{\partial^4\bar{\Sigma}}{\partial y^4} + c\frac{\partial}{\partial y}\left[\frac{\partial\bar{\Sigma}}{\partial y}\left(R\frac{\partial\bar{\theta}}{\partial y} - S\frac{\partial\bar{\Sigma}}{\partial y}\right)^2\right]. \tag{4}$$

The coefficients in this pair of equations are functions of the parameters, and are listed in the Appendix. They are calculated using the computer algebra package 'Mathematica'. These long-wave equations are more tractable than the full system (1), and, together with their counterparts for three-dimensional convection (to be introduced later), will be the subject of the remainder of this paper.

An equation similar to (4b) has been derived by Cessi and Young [28] in a model of the thermohaline circulation of the ocean. In that work, however, the temperature is specified at the upper boundary (so in our notation $\alpha_+ = \infty$), $\bar{\theta}$ is then a functional of $\bar{\Sigma}$, and does not evolve independently. Here the temperature and solute concentration play a more symmetrical role. Cessi [29] arrives at a pair of equations similar to (4) in a model for thermohaline convection on a β-plane. In both of these papers only steady convection is found as a large-time asymptotic state.

The qualitative nature of our results is independent of the choice of 'rigid-rigid' or 'free-free' boundary conditions for the streamfunction, although there are quantitative differences. Applying different boundary conditions on ψ at $z = 0$ than at $z = -1$, however, introduces new terms into (4) which break the odd symmetry $(\bar{\Sigma}, \bar{\theta}) \mapsto (-\bar{\Sigma}, -\bar{\theta})$. This circumstance is not considered further in this paper.

3.1. Linear stability

The linear growth rate, s, for small disturbances to the trivial solution $(\bar{\Sigma}, \bar{\theta}) = (0,0)$ in (4) satisfies the characteristic equation $s^2 - As + B = 0$, where

$$A = -(\alpha + \tau\gamma) + (\mathcal{R} - 1 - \tau(1+\mathcal{S}))k^2 - (a-b)k^4,$$
$$\tau^{-1}B = k^2[\alpha(1+\mathcal{S}) + \gamma(1-\mathcal{R})] + k^4[1 + \mathcal{S} - \mathcal{R}] + k^6(a - b/\tau) + \alpha\gamma + k^4(\gamma a - \alpha b/\tau).$$

In order to simplify these and later expressions we have introduced the scaled Rayleigh numbers $\mathscr{R} = dR$, and $\mathscr{S} = dS/\tau$, where d is recorded in the Appendix. We denote the two roots of the characteristic equation by s_1 and s_2. If, say, $s_2 < 0$ and s_1 passes through zero as $\mathscr{R}$ increases then a steady bifurcation occurs: the trivial solution becomes unstable to steady convection. This occurs when $B = 0$ with $A < 0$. An oscillatory (Hopf) bifurcation occurs if the real part of s_1 passes through zero with $\Im(s_1) = \Omega \neq 0$. In this case $s_2 = -s_1 = -i\Omega$. The Hopf bifurcation occurs when $A = 0$ with $B > 0$.

The widest rolls are stable according to the characteristic equation, as we see by examining the dominant terms in the limit as $k \to 0$. This gives $s^2 + (\alpha + \tau\gamma)s + \tau\alpha\gamma = 0$, whose roots, $s = -\alpha, -\tau\gamma$, are both negative. The narrowest rolls are also stable, provided the Rayleigh numbers are not too large: the dominant large-k terms in the characteristic equation are $s^2 + (a - b)k^4 s + (a - b/\tau)k^6 = 0$, and stability of the narrowest rolls corresponds to both $a - b$ and $a - b/\tau$ being positive. This is not the case for *all* values of the parameters, but is true near the onset of instability (see Appendix).

For the steady bifurcation, the critical Rayleigh number and critical wavenumber are, respectively,

$$\mathscr{R}_s = 1 + \mathscr{S} + 2[(\alpha(1 + \mathscr{S}) - \gamma\mathscr{S})(a_s - b_s/\tau)]^{1/2} + O(\epsilon^2)\,, \tag{5}$$

and

$$k_s = [(\alpha(1 + \mathscr{S}) - \gamma\mathscr{S})/(a_s - b_s/\tau)]^{1/4} + O(\epsilon)\,. \tag{6}$$

Since $\alpha, \gamma = O(\epsilon^2)$, $k_s = O(\epsilon^{1/2})$. The coefficients a_s and b_s are just a and b evaluated at $\mathscr{R} = 1 + \mathscr{S}$, instead of at $\mathscr{R} = \mathscr{R}_s = 1 + \mathscr{S} + O(\epsilon)$. In this way the expression for $\mathscr{R}_s$ is made explicit, at the expense of introducing small errors, which may be included in the terms of $O(\epsilon^2)$, $O(\epsilon)$ in (5), (6). For $\mathscr{R}_s$ and k_s to be real, we require $(\alpha(1 + \mathscr{S}) - \gamma\mathscr{S})(a_s - b_s/\tau) > 0$. We shall assume that this condition is satisfied. Since $a_s - b_s/\tau > 0$ (see Appendix) this inequality may be interpreted as placing an upper bound on γ, given α and $\mathscr{S}$: if γ is too large then the expansion (3), which assumes $\gamma = O(\epsilon^2)$, must be reconsidered.

For the Hopf bifurcation, the critical Rayleigh number and wavenumber are, respectively,

$$\mathscr{R}_o = 1 + \tau(1 + \mathscr{S}) + 2[(\alpha + \tau\gamma)(a_o - b_o)]^{1/2} + O(\epsilon^2)\,,$$

and

$$k_o = \left(\frac{\alpha + \tau\gamma}{a_o - b_o}\right)^{1/4} + O(\epsilon)\,,$$

where a_o and b_o are the coefficients a, b in (4) evaluated at $\mathscr{R} = 1 + \tau(1 + \mathscr{S})$ rather than at $\mathscr{R} = \mathscr{R}_o = 1 + \tau(1 + \mathscr{S}) + O(\epsilon)$, to make the expression for $\mathscr{R}_o$ explicit. To ensure that k_o and $\mathscr{R}_o$ are real we require $a_o - b_o > 0$ (verified in the Appendix). At the onset of instability $s_{1,2} = \pm i\omega k_o^2$, where $\Omega = \omega k_o^2$ is the frequency of the oscillations, and $\omega^2 = \tau(1 + \mathscr{S}) - \mathscr{R}\tau + O(\epsilon)$. Since ω^2 must be positive, the oscillatory bifurcation can happen only if $\mathscr{S} > \mathscr{S}_d$, where $\mathscr{S}_d = \tau/(1 - \tau) + O(\epsilon)$. By contrast, the steady bifurcation occurs as $\mathscr{R}$ is increased with $\mathscr{S} < \mathscr{S}_d$, so that the stabilizing vertical solute gradient is weak. This is reasonable on physical grounds, since a statically stable vertical concentration gradient acts as a restoring force for a vertically displaced fluid parcel; if this restoring force is weak then diffusive damping prevents overstability. We expect an oscillatory bifurcation if the vertical solute con-

centration gradient is strongly stabilizing, because then the restoring force on a vertically displaced fluid parcel can overcome diffusion, cause overshoot, and hence oscillations.

3.1.1. The onset of convection

Figure 3 compares the marginal curves according to the long-wave equations (4) with a numerical solution [7] of the linearized eigenvalue problem for (1). The expansion performs well in the limit as $k \to 0$, and around the critical wavenumber, but loses accuracy (as expected) for large k. A close examination of the numerically-computed eigenmodes for small k shows them to agree well with the expansion (3).

The first instability of the trivial solution is steady if $\mathcal{R}_s < \mathcal{R}_o$, and oscillatory otherwise. Near the point $\mathcal{S} = \mathcal{S}_d$, a simultaneous bifurcation to steady and oscillatory convection occurs, when $\mathcal{R}_s = \mathcal{R}_o \equiv \mathcal{R}_d$. In general, the critical wavenumbers k_s and k_o will differ, but for the numerical integrations of (4) we describe later, carried out in a finite box $0 \leq y \leq L$, the bifurcation at $(\mathcal{R}, \mathcal{S}) = (\mathcal{R}_d, \mathcal{S}_d)$ is of particular interest when $k_s = k_o$. The coincidence of critical wavenumbers can be achieved by a judicious choice of the ratio $\gamma/\alpha = (\gamma/\alpha)_d$. Equating k_s and k_o, we find we must take

$$\left(\frac{\gamma}{\alpha}\right)_d = \begin{cases} \dfrac{34 + 11/\sigma}{34 + 11\tau/\sigma} + O(\epsilon) & \text{('rigid-rigid')} \\ \dfrac{2182 + 561/\sigma}{2182 + 561\tau/\sigma} + O(\epsilon) & \text{('free-free')}. \end{cases}$$

If such a choice is made then at the onset of instability both eigenvalues of the characteristic equation vanish. The bifurcation is then a 'double-zero' or 'Takens–Bogdanov' bifurcation [30, 31], in whose neighbourhood the steady and oscillatory modes of convection compete.

3.2. Weakly non-linear results

We now summarize the weakly non-linear analysis of (4) near the steady, oscillatory and double-zero bifurcations: this analysis guides our numerical calculations (the details may be found in [21]).

Linear theory predicts that the onset of convection is steady if $0 < \mathcal{S} < \mathcal{S}_d$. A weakly non-linear expansion of the steady-state (SS) solution reveals that the steady bifurcation is supercritical if $0 \leq \mathcal{S} < \mathcal{S}^* = \tau^2/(1-\tau^2) + O(\epsilon)$, but subcritical if $\mathcal{S}^* < \mathcal{S} < \mathcal{S}_d$. In the first

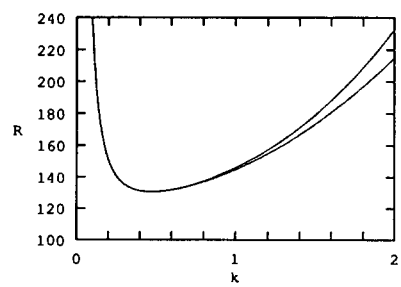

Fig. 3. Comparison of marginal curves for thermosolutal convection according to (1) – the upper curve – and the long-wave model (4) – the lower curve. The agreement between the two curves for small wavenumbers is excellent. Parameters are: $S = 0$, $\sigma = 7$, $\tau = 1/80$, $\gamma = 0$, $\alpha_{\pm} = 0.005$ (and 'free-free' boundaries).

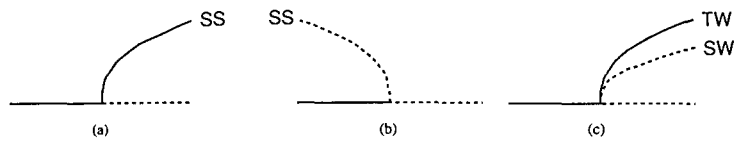

Fig. 4. Bifurcation diagrams for: (a) the supercritical steady bifurcation ($0 < \mathcal{S} < \mathcal{S}^*$); (b) the subcritical steady bifurcation ($\mathcal{S}^* < \mathcal{S} < \mathcal{S}_d$); (c) the oscillatory bifurcation ($\mathcal{S} > \mathcal{S}_d$). The thermal Rayleigh number R increases to the right, and stable solutions are indicated by solid lines (unstable solutions are dashed). SS, TW, SW represent, respectively, steady states, travelling waves and standing waves.

case the onset of convection as $\mathcal{R}$ is increased is gradual; in the second it is sudden. Bifurcation diagrams for the two cases are given in Fig. 4(a) and (b).

At the oscillatory bifurcation that occurs when $\mathcal{R} = \mathcal{R}_0$ and $\mathcal{S} > \mathcal{S}_d$, three branches of solutions emerge, all supercritical: one branch of standing waves (SW), together with left- and right-travelling waves (TW). The standing waves are unstable to travelling-wave perturbations, and each travelling wave is stable. A bifurcation diagram is given in Fig. 4(c).

An analysis of the double-zero bifurcation at $(\mathcal{R}, \mathcal{S}, \gamma/\alpha) = (\mathcal{R}_d, \mathcal{S}_d, (\gamma/\alpha)_d)$ captures both the subcritical steady bifurcation and the oscillatory bifurcation near $\mathcal{S} = \mathcal{S}_d$, and allows interaction between the different branches of solutions. Dangelmayr and Knobloch [31] have a catalogue of bifurcation diagrams which may be appropriate for different systems near a Takens–Bogdanov bifurcation. In our case, for $\mathcal{S}$ just below $\mathcal{S}_d$, Fig. 4(b) is appropriate, and as $\mathcal{R}$ is increased a subcritical branch of steady rolls emerges: there is no Hopf bifurcation. On the other hand, for $\mathcal{S}$ just above $\mathcal{S}_d$, Fig. 5 applies, and we expect a more complicated transition as $\mathcal{R}$ is increased. First the trivial solution of (4) becomes unstable in a Hopf bifurcation to TW and SW (as in Fig. 4(c)). The SW are unstable and the TW are initially stable. However, the TW lose stability in a Hopf bifurcation to modulated travelling waves (MW). These MW are travelling waves with a periodic modulation of their amplitude. They in turn are destroyed in a heteroclinic bifurcation with the SW as $\mathcal{R}$ is further increased. Thereafter the SW are stable until they disappear at a heteroclinic bifurcation with the small-amplitude subcritical SS. For larger values of $\mathcal{R}$ none of the small-amplitude solutions predicted by the weakly non-linear theory is stable and the solution is attracted to a

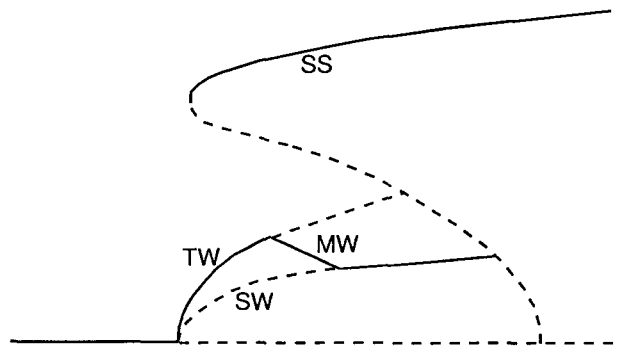

Fig. 5. Bifurcation diagram for the double-zero bifurcation at $(\mathcal{R}, \mathcal{S}) \sim (\mathcal{R}_d, \mathcal{S}_d)$. As $\mathcal{R}$ is increased (with $\mathcal{S}$ just above $\mathcal{S}_d$) the stable states are successively: trivial solution; travelling waves (TW); modulated waves (MW); standing waves (SW). After the connection of the standing wave branch with the subcritical steady branch (SS), none of the small-amplitude solutions is stable, and the solution of (4) appears, on the basis of our numerical integrations, always to asymptote to the large-amplitude steady solution (this solution is indicated here, but is not strictly a prediction of the weakly non-linear theory).

large-amplitude SS (which appears to be globally attracting, on the basis of numerical integrations of the initial-value problem for (4)).

4. Comparison between the long-wave limit and ideal double diffusion

It is interesting to compare the linear and weakly non-linear results described above with those for ideal double diffusion ('IDD'), that is, where the governing equations are (1), boundary conditions are 'free-free', and $\theta = \Sigma = 0$ at $z = 0, -1$. IDD can be treated analytically, and we make our comparison with the results of Huppert and Moore [3]. It turns out that apart from numerical factors IDD and the long-wave limit described here are quite similar.

(i) The critical wavenumber in IDD is $\pi/\sqrt{2}$, where our critical wavenumber depends on the parameters (albeit weakly, except for a strong dependence on $\alpha_{\pm}$, when $\alpha_{\pm}$ are small). (ii) The bifurcations of the basic state in IDD as R is increased are: supercritical steady ($0 < S < S^*$); subcritical steady ($S^* < S < S_d$); supercritical oscillatory ($S_d < S < S_{bi}$); subcritical oscillatory ($S_{bi} < S$). Our expansion contains the first three but not the last; our theory is not valid for sufficiently large Rayleigh numbers. (iii) The value of S separating supercritical and subcritical steady bifurcations is $S^* = m\tau^3/(1-\tau^2)$, where for IDD $m = 27\pi^4/4 \approx 657.511$ and here $m = 1/d + O(\epsilon)$. (iv) The value of S separating steady and oscillatory bifurcations for IDD is $S_d = m\tau^2/(1-\tau)$, with $m = (27\pi^4/4)(1 + 1/\sigma)$. For the present problem, the separating value is not so clear because the critical wavenumbers of the steady and the oscillatory bifurcations may differ, but $S_d = m\tau^2/(1-\tau) + O(\epsilon)$, where $m = 1/d$. The absence of σ in our expression for m may be attributed to the late appearance of ψ in the asymptotic expansion (3). (v) A significant difference between the present problem and IDD is that in IDD the bifurcation of the travelling wave branch is degenerate, and its direction cannot be determined from the cubic-order Landau equations. Here, there is no such degeneracy, and the cubic-order weakly non-linear theory predicts stable supercritical travelling waves. The non-degenerate bifurcation to TW also allows us *rigorously* to apply the theory of Dangelmayr and Knobloch [31] near the double-zero point.

Another interesting comparison is with the long-wave theory [17, 19] for Rayleigh–Bénard convection, obtained here by setting $S = 0$. In that case the convection is governed by a single PDE for $\bar{\theta}$. Provided that symmetric boundary conditions are applied to the streamfunction at top and bottom, this long-wave equation has a Lyapunov functional, and so the long-time behaviour of solutions must be time-independent. No such Lyapunov functional exists for (4): we can demonstrate the existence of stable oscillatory modes of convection according to the weakly non-linear theory (and find then numerically – see the next section).

5. Spectral simulations

We have computed solutions of the long-wave equations (4) under 'free-free' boundary conditions using a spectral code, near the steady, double-zero and oscillatory bifurcations. We apply periodic lateral boundary conditions, with spatial period L. The solutions are expanded as Fourier series:

$$\bar{\theta} = \sum_{n=-\infty}^{\infty} \theta_n(t)\, e^{inky}, \qquad \bar{\Sigma} = \sum_{n=-\infty}^{\infty} \Sigma_n(t)\, e^{inky},$$

where $k = 2\pi/L$, and these expansions are substituted into (4), resulting in ODEs for the amplitudes θ_n, Σ_n. Without loss of generality for long-time integrations we set $\theta_0 = \Sigma_0 = 0$. The ODEs are truncated at $n = N$, say: we have generally chosen $N = 15$, which gives reliable and accurate results. For example, with only $N = 9$ modes spurious period-doubling to chaos is observed on the branch of modulated waves. The ODEs are integrated using the NAG routine d02eaf, a variable-order, variable-step solver for stiff systems. Some of the checks we have performed on the numerical code are described in the Appendix.

We have not attempted an exhaustive numerical investigation of parameter space for (4), but we expect our results to be representative. Our numerical protocol varies R, with all other parameters fixed. We have chosen to examine two sets of values for the Prandtl and Lewis numbers: (i) $\sigma = 7$ and $\tau = 1/80$, appropriate for the oceanographic problem of the diffusion of salt and heat in water [3, 2]; and (ii) $\sigma = 1$ and $\tau = 1/6.7$, appropriate for the Langmuir circulation problem [7, 8, 10, 11]. We have chosen to set $\alpha = 0.01$, so that the small parameter $\epsilon \sim 0.1$. The value for γ ensures that $k_s = k_0$ when $R_s = R_0$: (i) $\gamma = 0.01 \times (\gamma/\alpha)_d \approx 0.0104$; (ii) $\gamma = 0.01 \times (\gamma/\alpha)_d \approx 0.0121$.

(I) Thermohaline convection

For each value of S the critical wavenumber will be different, but over the range of S that we investigate k_c varies by less than 5%, and so we fix $L = 2\pi/k$ for all our integrations, where $k = 0.474733$, which is approximately the critical wavenumber at the double-zero point.

With the salt/heat-in-water application in mind, we find that $S^* \approx 2.3 \times 10^{-4}$, so that only for very small values $S < S^*$ is the steady bifurcation supercritical. Furthermore $S_d \approx 0.019$, so only for S less than this value is the instability of the trivial solution steady, rather than oscillatory.

When $S = 0$, so that the salt plays a passive role, the weakly non-linear theory predicts a supercritical bifurcation to steady convection. Our numerical integrations of (4) agree well with this prediction, and in Fig. 6 we show our numerical results, together with the prediction of weakly non-linear theory (CL).

The computations reveal an unfortunate feature of the model (4) for large values of R. The amplitude of convection, after first increasing monotonically with R, then starts to diminish as R is further increased (Fig. 7). Eventually, the trivial solution becomes stable,

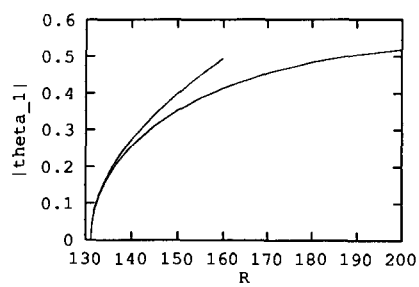

Fig. 6. The lower curve is a plot of $|\theta_1|$ against R computed numerically for thermohaline convection. The upper curve is the weakly non-linear prediction, valid in the limit as $R \to R_c \approx 131.17$. Here $\mathcal{S} = 0$.

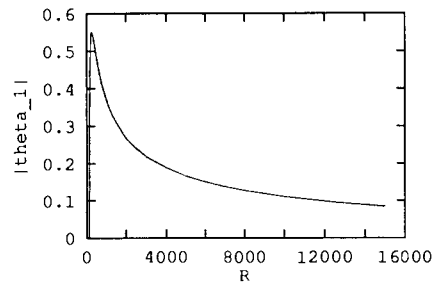

Fig. 7. Same as Fig. 6, except for the extended range of thermal Rayleigh number, showing the incorrect large-R behaviour of the long-wave model (4), that the convection becomes weak for large R (and for large enough R, not shown here, the trivial solution restabilizes).

and appears from the numerical integrations to be globally attracting. Such behaviour is a consequence of the long-wave model (4), and does not reflect the true behaviour of (1), where an increasing range of wavenumbers is destabilized as R is increased. We investigate this discrepancy in a later section. For now it is sufficient to note that large-R (and large-S) behaviour of (4) does not correspond to true behaviour of (1). Therefore no large-R or large-S numerical results for (4) are reported here.

Numerical results for $S = 1/100 > S^*$ are indicated in Fig. 8. Here the subcritical branch of steady solutions predicted by weakly non-linear theory is included, although this branch is unstable, and cannot be computed using our time-dependent code.

For $S = 1 > S_d$ the linear theory predicts a Hopf bifurcation of the trivial solution as R is increased through R_0. In agreement with the weakly non-linear predictions, we find branches of travelling waves (TW) and standing waves (SW) for $R > R_0$, with the TW stable and the SW unstable (Fig. 4(c)). A summary of the numerical results is given in Fig. 9.

The SW are not indicated in the figure, although we have computed them for a few values of R, by choosing a small-amplitude initial condition with reflection symmetry in the plane $y = 0$. When, subsequently, we add a perturbation to the fully-developed SW that breaks the reflection symmetry, this perturbation grows until the SW is lost, and the solution tends to either the TW or the large-amplitude SS. All SW we have computed have turned out to be unstable to such perturbations. Standing waves in finite-wavenumber thermosolutal convection have been examined by Schöpf and Zimmermann [32], Knobloch and Moore [33] (both according to linear theory), and by Cox et al. [8] for Langmuir circulation (according to weakly non-linear theory and numerical simulation), and found to have a vertical structure that changes according to the phase of the SW cycle. In contrast, the present SW have a

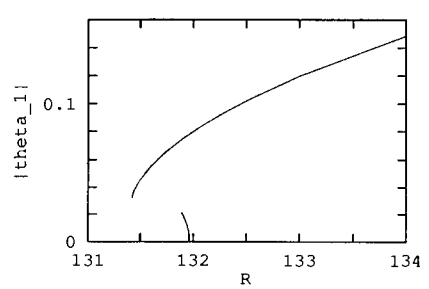

Fig. 8. Numerical results for thermohaline convection at $S = 1/100$: plot of $|\theta_1|$ against R. Upper curve is the large-amplitude steady branch; lower solid curve is the weakly non-linear prediction for the unstable subcritical steady branch which links the bifurcation point to the turning point of the large-amplitude solutions.

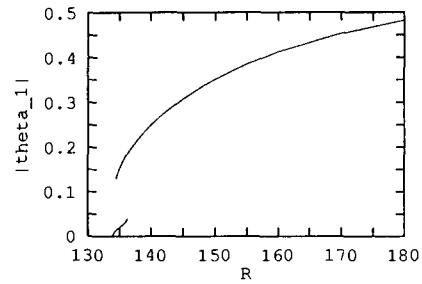

Fig. 9. Numerical results for thermohaline convection at $S = 1$: plot of $|\theta_1|$ against R. Upper curve is the large-amplitude steady-state branch; lower curve is the travelling wave branch.

constant vertical structure, because ψ is a separable function of y and z, at least if the streamfunction is reconstructed from ψ_1 alone, once $\bar{\theta}$ and $\bar{\Sigma}$ are computed.

Numerical integrations near the double-zero bifurcation failed to yield any solution other than the large-amplitude steady state branch. We attribute the apparent lack of oscillatory solutions (which should exist, as in Fig. 5) to our not integrating sufficiently close to the double-zero point (R_d, S_d). With high precision and enormous patience we could no doubt find TW, SW and MW there.

(II) Langmuir circulation

With $\sigma = 1$ and $\tau = 1/6.7$, appropriate for Langmuir circulation, the critical wavenumber is only weakly dependent on S, and we fix $L = 2\pi/k$, with the double-zero value $k \approx 0.47034$. The significant values for S are: $S^* \approx 0.408$, $S_d \approx 3.142$.

The same qualitative picture emerges here as for (i), except we have been able to capture the oscillatory solutions near the double-zero bifurcation. Figures 10 and 11 present our numerical results for $S = 10$ and $S = 20$, respectively. Stable travelling waves and modulated waves are found, in accordance with the predictions based around the double-zero point (Fig. 5), even though S is quite far removed from S_d. These oscillatory solutions co-exist with the large-amplitude steady state. Stable standing waves are found, albeit in a very small parameter range: for example, when $S = 4$ stable standing waves are found for values of R between approximately 156 and 156.145.

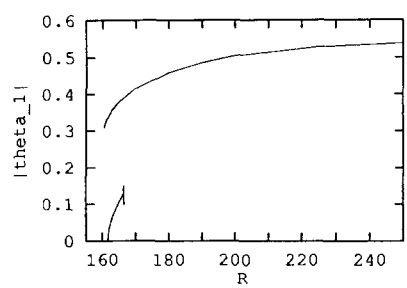

Fig. 10. Numerical results for Langmuir circulation with $S = 10 > S_d$. Upper curve is the branch of steady states; lower curve is the travelling wave branch, which bifurcates into modulated waves at $R \approx 166.5$. The MW have an oscillatory amplitude, and the figure indicates the maximum and minimum values of $|\theta_1|$ during the MW cycle. The TW and MW co-exist with the SS.

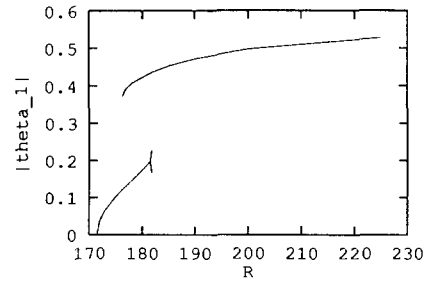

Fig. 11. As for Fig. 10, except $S = 20$. The TW and MW branches grow to larger amplitude than for $S = 10$, and now there is a region near the onset of the TW where the TW are the only stable state.

6. Large-$\mathscr{R}$ asymptotics

Our numerical results show that the behaviour of (4) in the limit of large $\mathscr{R}$ (or R) does not reflect that of (1). According to the long-wave theory the motionless state is stable for large $\mathscr{R}$, whereas in fact it should be increasingly unstable. This discrepancy arises because the asymptotic expansion (3) becomes disordered as $\mathscr{R}$ becomes large – an examination of the terms in the small-ϵ expansion (3) reveals that for large $\mathscr{R}$

$$(\theta, \Sigma, \epsilon^{-1/2}\mathscr{R}^{-1}\psi) = O(1) + O(\epsilon\mathscr{R}) + O(\epsilon^2\mathscr{R}^2) + \cdots,$$

so the expansion is useful only if $\epsilon\mathscr{R} \ll 1$. It cannot, therefore, be the basis for an investigation of the large-$\mathscr{R}$ behaviour of (1) for fixed, but small, wavenumber (that is, for fixed ϵ). Physically, when $\mathscr{R}$ is not large the convective motions are sufficiently weak that vertical diffusion of θ and Σ can maintain these fields in an almost depth-independent state, assumed in (3). For larger values of $\mathscr{R}$, convection is more vigorous and the vertical homogeneity of θ and Σ cannot be maintained by vertical diffusion against strong advection.

In (1) the unstable wavenumbers lie between $k_{\min} = O(\mathscr{R}^{-1/2})$ and $k_{\max} = O(\mathscr{R}^{1/4})$, so that as $\mathscr{R}$ is increased, an increasing interval of wavenumbers is unstable. Not all these unstable eigenmodes are captured well by the small-k analysis that leads to (4). In particular our numerical solutions of the linear stability problem for (1) indicate that the vertical structure of the θ- and Σ-components of the eigenmodes of (1) is not even approximately homogeneous when $\mathscr{R}$ is large. Furthermore, for large $\mathscr{R}$ and $k = O(1)$ the most unstable eigenmode has θ and Σ *smaller* than ψ by a factor of $\mathscr{R}^{1/2}$, so the ordering assumed in (3), that θ and Σ dominate ψ, becomes invalid.

7. Three-dimensional convection

In the Appendix we sketch an expansion to reduce three-dimensional convection to two dimensions in the long-wave limit. The simplest case, and the only one treated here, is that of infinite Prandtl number and 'rigid-rigid' boundaries. With x and y the horizontal coordinates, the analogue of (4) for three-dimensional convection is

$$\begin{aligned}\frac{\partial\bar{\theta}}{\partial t} &= -\alpha\bar{\theta} + \nabla_H^2[\bar{\theta} + d(S\bar{\Sigma} - R\bar{\theta})] - a\nabla_H^4\bar{\theta} + b\nabla_H^4\bar{\Sigma} \\ &\quad + \tau c\nabla_H \cdot \{[\nabla_H(R\bar{\theta} - S\bar{\Sigma}) \cdot \nabla_H\bar{\theta}]\nabla_H(R\bar{\theta} - S\bar{\Sigma})\},\end{aligned} \tag{7}$$

$$\frac{\partial \bar{\Sigma}}{\partial t} = -\tau\gamma\bar{\Sigma} + \nabla_H^2[\tau\bar{\Sigma} + d(S\bar{\Sigma} - R\bar{\theta})] - a\nabla_H^4\bar{\theta} + b\nabla_H^4\bar{\Sigma}$$
$$+ c\nabla_H \cdot \{[\nabla_H(R\bar{\theta} - S\bar{\Sigma}) \cdot \nabla_H\bar{\Sigma}]\nabla_H(R\bar{\theta} - S\bar{\Sigma})\} .$$

Here $\bar{\theta} = \bar{\theta}(x, y, t)$, $\bar{\Sigma} = \bar{\Sigma}(x, y, t)$, and the gradient operator is $\nabla_H \equiv (\partial_x, \partial_y)$. We shall analyse the onset of convection according to (7) in a square periodic geometry with $0 < x, y < 2\pi/k_c$.

7.1. *Steady bifurcation*

Near the supercritical steady bifurcation, as $\mathscr{R}$ is increased with $0 < \mathscr{S} < \mathscr{S}^*$, there is competition between rolls and squares. (Squares are the non-linear counterpart of a linear superposition of rolls oriented at right angles.) Busse and Riahi [24] demonstrated that squares are stable, and rolls unstable to cross-roll perturbations for long-wave Rayleigh–Bénard convection. Their results rely on the Lyapunov functional which exists in that problem, and we cannot apply their technique to the present problem because the pair of equations (7) possess no such Lyapunov functional. Knobloch [22] has used equivariant bifurcation theory to predict a range of outcomes for the competition between squares and rolls in long-wave convection, according to the values of various coefficients. His analysis proceeds from a single long-wave equation, such as arises in Rayleigh–Bénard convection, rather than the pair we have here, but he does not assume the existence of a Lyapunov functional.

For the present problem we derive coupled Landau equations for the amplitudes of rolls oriented a right-angles, and calculate the stability of the roll and square solutions directly. Near the steady bifurcation, with $\mathscr{R} = \mathscr{R}_s + \delta^2\mathscr{R}_2$, we let the solution be

$$\bar{\theta} = \delta(A^{(x)}(t)\, e^{ik_c x} + A^{(y)}(t)\, e^{ik_c y}) + \text{c.c.} + O(\delta^3)$$
$$\bar{\Sigma} = \delta(mA^{(x)}(t)\, e^{ik_c x} + mA^{(y)}(t)\, e^{ik_c y}) + \text{c.c.} + O(\delta^3) ,$$

where $m = 1/\tau + O(\epsilon)$, and substitute this expansion into (7), considering successive (odd) powers of the expansion parameter, δ. The amplitudes $A^{(x)}$ and $A^{(y)}$ are associated with roll solutions perpendicular to the x- and y-axes, respectively, and evolve on the slow time scale $\delta^2 t$. At $O(\delta^3)$ we find coupled Landau equations for the amplitudes of the x- and y-rolls,

$$\frac{dA^{(x)}}{dt} = A^{(x)}[\mu_1\mathscr{R}_2 - \mu_2(|A^{(x)}|^2 + \tfrac{2}{3}|A^{(y)}|^2)]$$
$$\frac{dA^{(y)}}{dt} = A^{(y)}[\mu_1\mathscr{R}_2 - \mu_2(\tfrac{2}{3}|A^{(x)}|^2 + |A^{(y)}|^2)] ,$$

where

$$\mu_1 = \frac{\mathscr{S}_d k_s^2}{\mathscr{S}_d - \mathscr{S}} > 0 , \qquad \mu_2 = \frac{3c\tau|\mathscr{S}^* - \mathscr{S}|k_s^4\mathscr{S}_d}{d^2\mathscr{S}^*(\mathscr{S}_d - \mathscr{S})} + O(\epsilon^3) > 0 .$$

We discuss only the supercritical steady bifurcation ($0 < \mathscr{S} < \mathscr{S}^*$), where $\mu_2 > 0$. (For $\mathscr{S} > \mathscr{S}^*$ the sign of μ_2 is reversed, and the bifurcation is subcritical. Then fifth-order terms must be included in the Landau equations in order for the amplitudes to saturate.)

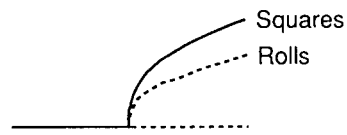

Fig. 12. Bifurcation diagram for steady three-dimensional convection in a square geometry. Branches of rolls parallel to each horizontal coordinate axis emerge as $\mathscr{R}$ is increased, together with a branch of squares. The rolls are unstable, and the squares stable.

When $\mathscr{R}_2 < 0$ the only steady-state solution is the zero solution, which is stable. It becomes unstable for $\mathscr{R}_2 > 0$, and two branches of steady rolls emerge, with $(|A^{(x)}|^2, |A^{(y)}|^2) = (\mu_1\mathscr{R}_2/\mu_2, 0)$ or $(0, \mu_1\mathscr{R}_2/\mu_2)$, together with a branch of squares, with $|A^{(x)}|^2 = |A^{(y)}|^2 = 3\mu_1\mathscr{R}_2/5\mu_2$. All branches are supercritical, that is, they exist for $\mathscr{R}_2 > 0$, with squares stable and rolls unstable to cross-roll perturbations. A bifurcation diagram is given in Fig. 12.

7.2. *Hopf bifurcation*

The long-wave Hopf bifurcation does not seem to have been studied previously in convection problems. Near the Hopf bifurcation, with $\mathscr{R} = \mathscr{R}_0 + \delta^2\mathscr{R}_2$, the leading-order solution is a superposition of four travelling waves which bifurcate simultaneously, one in each sense parallel to each axis:

$$\begin{aligned}\bar{\theta} &= \delta(A^{(x,r)}\,e^{i(k_c x-\Omega t)} + A^{(x,l)}\,e^{i(k_c x+\Omega t)} \\ &\quad + A^{(y,r)}\,e^{i(k_c y-\Omega t)} + A^{(y,l)}\,e^{i(k_c y+\Omega t)}) + \text{c.c.} + O(\delta^3) \\ \bar{\Sigma} &= \delta(mA^{(x,r)}\,e^{i(k_c x-\Omega t)} + m^*A^{(x,l)}\,e^{i(k_c x+\Omega t)} \\ &\quad + mA^{(y,r)}\,e^{i(k_c y-\Omega t)} + m^*A^{(y,l)}\,e^{i(k_c y+\Omega t)}) + \text{c.c.} + O(\delta^3)\,.\end{aligned}$$

After a good deal of algebra, we find the coupled Landau equations that govern the four amplitudes to be

$$\frac{\mathrm{d}}{\mathrm{d}t}|A^{(x,r)}| = |A^{(x,r)}|[\mu_3\mathscr{R}_2 - \mu_4(|A^{(x,r)}|^2 + 2|A^{(x,l)}|^2 + 2|A^{(y,r)}|^2 + 2|A^{(y,l)}|^2)]\,, \tag{8}$$

and its three cyclical counterparts, where to leading order in ϵ, $\mu_3 = k_0^2/2$, and $\mu_4 = ck_0^4(1-\tau^2)\mathscr{R}_0/(2d^2)$.

There are five classes of steady-state solutions to the governing equations indicated in (8), according to the number of amplitudes that are non-zero.

Firstly the zero solution, where all amplitudes vanish, is stable for $\mathscr{R}_2 < 0$ and unstable for $\mathscr{R}_2 > 0$. The four other classes of solution bifurcate supercritically from zero as $\mathscr{R}$ increases through $\mathscr{R}_0$. There are four travelling-wave solutions, for example

$$|A^{(x,r)}|^2 = \mu\,, \qquad |A^{(x,l)}| = A^{(y,r)}| = |A^{(y,l)}| = 0\,,$$

where we define $\mu = \mu_3\mathscr{R}_2/\mu_4$. By linearizing about this steady state we find the eigenvalues associated with infinitesimal disturbances to be $(-2\mu, -\mu, -\mu, -\mu)$; since all are negative then each TW is stable. There are six two-mode solutions, for example

$$|A^{(x,r)}|^2 = |A^{(x,l)}|^2 = \mu/3\,, \qquad |A^{(y,r)}| = |A^{(y,l)}| = 0\,. \tag{9}$$

All six are equivalent according to the amplitude equations even though some, like (9), represent standing waves, while others represent mixed x-TW and y-TW states. In each case the eigenvalues of the linearization about the steady state are $(-2\mu, 2\mu/3, -\mu/3, -\mu/3)$, and these states are unstable to perturbations which amplify either of their two non-zero components. There are four three-mode solutions, again all equivalent, for example

$$|A^{(x,r)}|^2 = |A^{(x,l)}|^2 = |A^{(y,r)}|^2 = \mu/5\,, \qquad |A^{(y,l)}| = 0\,.$$

The eigenvalues of this state are $(-2\mu, 2\mu/5, 2\mu/5, -\mu/5)$, and the dangerous perturbations drive the system to a single-mode TW solution. Finally, there is the full four-mode mixed-SW state, with

$$|A^{(x,r)}|^2 = |A^{(x,l)}|^2 = |A^{(y,r)}|^2 = |A^{(y,l)}|^2 = \mu/7\,.$$

This solution has the eigenvalues $(-2\mu, 2\mu/7, 2\mu/7, 2\mu/7)$, and so is unstable. In summary, for supercritical conditions ($\mathscr{R}_2 > 0$) the only stable steady-state solutions of the amplitude equations (8) represent two-dimensional TW solutions.

8. Conclusion

The long-wave results we have described for two-dimensional convection mirror the bifurcations of the basic state in IDD: the instability is steady when the restoring force due to the vertical solute gradient is weak, and oscillatory when it is stronger; at first the steady bifurcation is supercritical, then subcritical for larger solutal Rayleigh numbers; travelling waves are the preferred mode of oscillatory convection. The quantitative details differ, but the qualitative story is the same.

In contrast to the long-wave theory for Rayleigh–Bénard convection [17, 19], the long-wave equations presented here for thermosolutal convection do not possess a Lyapunov functional, and there are stable oscillatory solutions (primarily travelling waves). In our derivation of the pair of long-wave equations (4) we have assumed that γ is small: if this is not so then a single long-wave equation is appropriate for $\bar{\theta}$ [34], and it has a Lyapunov functional [35].

Our numerical simulations reproduce all stable states predicted by weakly non-linear theory, and continue these solutions beyond the regions in parameter space where small-amplitude expansions are valid, near bifurcation points. Over-all, the only solutions of (4) likely to be observed are the steady states and the travelling waves, and these states may co-exist over small ranges of parameters. Standing waves and modulated waves are confined to tiny regions of parameter space (indeed we could not find them at all for thermohaline convection, these regions were so small).

The long-wave expansion is useful not too far above onset, but it is inappropriate for large Rayleigh numbers since the terms in the expansion become disordered. This restriction does not result from an assumption that the solutions are of small amplitude, rather that the convection should take a particular form, with the temperature and solute concentration fields approximately vertically uniform. Such a diffusion-dominated structure cannot be maintained against vigorous convective motions.

The two-dimensional rolls that arise at the supercritical steady bifurcation for $0 < \mathscr{S} < \mathscr{S}^*$

are unstable to cross-roll perturbations, at least near their onset, and so we would not expect to find them in a square geometry. This result agrees with that of a long-wave analysis for Rayleigh–Bénard convection [19, 22]. A square planform is the preferred mode of steady convection in that case. We have not determined whether the large-amplitude steady-states are similarly unstable, and so whether these rolls might be observable in the three-dimensional problem. The two-dimensional travelling waves are stable to parallel and to perpendicular disturbances, and so are the preferred form for three-dimensional oscillatory convection.

Acknowledgements

The author is an Australian Research Council Australian Postdoctoral Research Fellow.

Appendix

A. Appendix

A.1. Coefficients of (4)

The coefficients of (4) given by the following expressions:

$$a = \frac{\mathscr{R}}{\beta_1}\{\beta_2(\mathscr{S} - \mathscr{R}) + \beta_3[2 - 1/\sigma + (\mathscr{R} - \tau\mathscr{S})/\sigma]\}$$

$$b = \frac{\tau\mathscr{S}}{\beta_1}\{\beta_2(\mathscr{S} - \mathscr{R}) + \beta_3[2 - \tau/\sigma + (\mathscr{R} - \tau\mathscr{S})/\sigma]\},$$

where $\beta_1 = 462$, $\beta_2 = 5$, $\beta_3 = 11$, $c = 1/(362880\tau)$, $d = 1/720$ for the 'rigid-rigid' case, and $\beta_1 = 5544$, $\beta_2 = 31$, $\beta_3 = 561$, $c = 31/(362880\tau)$, $d = 1/120$ for the 'free-free' case. In each case $\mathscr{R} = dR$ and $\mathscr{S} = dS/\tau$.

The weakly non-linear calculations near the steady and the Hopf bifurcations require $a - b/\tau > 0$ and $a - b > 0$, respectively. Although these inequalities certainly do not hold for all choices of the parameters $\mathscr{R}$, $\mathscr{S}$, σ, τ, they do hold close to the bifurcation point. Near the steady bifurcation $a - b/\tau = 17/462 + O(\epsilon)$ ('rigid-rigid'), or $a - b/\tau = 1091/5544 + O(\epsilon)$ ('free-free'), and so when ϵ is small $a - b/\tau > 0$. Near the Hopf bifurcation we find

$$a - b = [17(1 + \tau) + 11\tau/\sigma]/462 + O(\epsilon) > 0 \quad \text{('rigid-rigid')},$$
$$a - b = [1091(1 + \tau) + 561\tau/\sigma]/5544 + O(\epsilon) > 0 \quad \text{('free-free')}.$$

When ϵ is small $a - b > 0$.

A.2. Checks on the numerical code

We have checked the numerical calculations of steady and unsteady motions in (4) in several ways. We have compared the growth rates and decay rates of small disturbances with those predicted by linear theory, and find excellent agreement. Quantitative checks have also been made against the weakly non-linear theory [21], both for travelling waves and for steady states, and are indicated in Table 1.

Table 1. A comparison of numerical integrations of (4) using 15 modes ($N = 15$) and weakly non-linear theory with $\sigma = 7$, $\tau = 1/80$. All are for 'free-free' boundaries. The first table concerns the steady bifurcation with $S = 0$, where $R_s \approx 131.17$. The second concerns the TW at the Hopf bifurcation with $S = 1$, where $R_0 \approx 133.92$. The difference between the prediction and the numerics (given in the column marked 'Error') should tend to zero as $R \to R_c -$, and as $\epsilon \to 0$. (In these examples $\alpha = 0.01$, so $\epsilon \sim 0.1$.)

	$\lvert\theta_1\rvert$ WNL	$\lvert\theta_1\rvert$ Numerical	Error
$R = 131.3$	0.0336	0.0330	2%
$R = 132.0$	0.0839	0.0814	3%
$R = 135.0$	0.1800	0.1723	5%

	$\lvert\theta_1\rvert$ WNL	$\lvert\theta_1\rvert$ Numerical	Error
$R = 134.5$	0.01351	0.01409	4%
$R = 135.3$	0.02125	0.02266	6%
$R = 136.0$	0.0268	0.0319	17%

Most integrations described in Table 1 have used $N = 15$ modes. A reduction to $N = 9$ modes yields a significant reduction in computing times, and solutions are generally quite accurate, except for the MW, which undergo an interesting but spurious period-doubling cascade to chaos.

B. Derivation of (7)

The derivation of (7) proceeds by substitution of a small-ϵ expansion of the unknowns into the dimensionless equations governing the perturbations in three-dimensional convection:

$$\sigma^{-1}\left(\frac{\partial \mathbf{u}}{\partial t} + \mathbf{u}\cdot\nabla\mathbf{u}\right) = -\nabla p + (R\theta - S\Sigma)\mathbf{k} + \nabla^2\mathbf{u}$$

$$\frac{\partial \theta}{\partial t} + \mathbf{u}\cdot\nabla\theta + w = \nabla^2\theta$$

$$\frac{\partial \Sigma}{\partial t} + \mathbf{u}\cdot\nabla\Sigma + w = \tau\nabla^2\Sigma\,,$$

where $\mathbf{k}$ is the unit vertical. We expand $(\epsilon^{1/2}\mathbf{u}, \theta, \Sigma, p)$ as asymptotic series in powers of ϵ. The horizontal scale of the motions is $\epsilon^{-1/2}(x, y)$. The derivation below broadly follows the derivation of two-dimensional equations (1) by Cox and Leibovich [21], but here we may not employ a streamfunction. Furthermore, only 'rigid-rigid' boundaries and an infinite Prandtl number are considered – otherwise a large-scale pressure field drives a divergence-free velocity field that advects the temperature and concentration fields, which alters the form of the governing equations derived here.

At leading order in the expansion we find that θ_0 and Σ_0 are independent of the depth z. To avoid ambiguity, these quantities may be defined as the depth averages of θ and Σ, respectively. The leading-order pressure field serves to balance the buoyancy in the z-momentum equation: $p_0 = (z + 1/2)Y$, where $Y = R\theta_0 - S\Sigma_0$. The leading-order horizontal velocity field driven by this pressure is $(u_1, v_1) = (z^3/6 + z^2/4 - 1/24)\nabla_H Y$. The first contribution to the vertical velocity field, w_1, follows from the continuity equation: $w_1 = (z^4/24 + z^3/12 - z/24)\nabla_H^2 Y$.

At $O(\epsilon)$ in the governing equations we find evolution equations for θ_0, Σ_0 on the timescale ϵt: $\partial\theta_0/\partial t = \nabla_H^2(\theta_0 - dY)$, $\partial\Sigma_0/\partial t = \nabla_H^2(\tau\Sigma_0 - dY)$, where $d = 1/720$. Expressions for θ_1, Σ_1

are of the form $\theta_1 = \nabla_H Y \cdot \nabla_H \theta_0 D(z) + \nabla_H^2 Y E(z)$, $\Sigma_1 = \tau^{-1} \nabla_H Y \cdot \nabla_H \Sigma_0 D(z) + \tau^{-1} \nabla_H^2 Y E(z)$, where the polynomials D and E are found by solving inhomogeneous ordinary differential equations subject to zero-flux boundary conditions at upper and lower surfaces.

The pressure p_1 is determined from the z-momentum equation up to a function of integration, independent of depth:

$$p_1 = \nabla_H Y \cdot \nabla_H Z F(z) + [(R - S/\tau)G(z) - B(z)]\nabla_H^2 Y + \tilde{p}_1(x, y, t) .$$

The velocity components (u_2, v_2) may then be determined, up to terms proportional to $\tilde{p}_1$:

$$(u_2, v_2) = \nabla_H \{\nabla_H Y \cdot \nabla_H Z J(z) + [(R - S/\tau)K(z) - 2H(z)]\nabla_H^2 Y + \tilde{p}_1 L(z)\} .$$

The term $\tilde{p}_1$ is fixed once the depth-average of the continuity equation is considered at $O(\epsilon^2)$, whence

$$\overline{L(z)}\tilde{p}_1 = -\nabla_H Y \cdot \nabla_H Z \overline{J(z)} - [(R - S/\tau)\overline{K(z)} - 2\overline{H(z)}]\nabla_H^2 Y .$$

Now w_2 may be calculated from the continuity equation:

$$w_2 = -\nabla_H^2 \{\nabla_H Y \cdot \nabla_H Z N(z) + [(R - S/\tau)P(z) - 2M(z)]\nabla_H^2 Y + \tilde{p}_1 Q(z)\} .$$

The evolution equations for θ_0, Σ_0 on the slower time scale $\epsilon^2 t$ follow from a z-integration of the governing equations for θ and Σ:

$$\frac{\partial \theta_0}{\partial t} + \overline{(\mathbf{u}_1 \cdot \nabla_H + w_1 \partial_z)\theta_1} + \overline{\mathbf{u}_2 \cdot \nabla_H \theta_0} = \overline{w_4} - \alpha \theta_0$$

$$\frac{\partial \Sigma_0}{\partial t} + \overline{(\mathbf{u}_1 \cdot \nabla_H + w_1 \partial_z)\Sigma_1} + \overline{\mathbf{u}_2 \cdot \nabla_H \Sigma_0} = \overline{w_4} - \tau\gamma \Sigma_0 .$$

The result is the pair (7), where we use the fact that the following polynomials are odd in $z + 1/2$, and so have zero average over the depth: B, D, G, H, K, N, Q, T.

References

1. H. Stommel, A.B. Arons and D. Blanchard, An oceanographic curiosity: the perpetual salt fountain. *Deep-Sea Research* 3 (1956) 152–153.
2. G. Veronis, Effect of a stabilizing gradient of solute on thermal convection. *J. Fluid Mech.* 34 (1968) 315–336.
3. H.E. Huppert and D.R. Moore, Non-linear double-diffusive convection. *J. Fluid Mech.* 78 (1976) 821–852.
4. M.R.E. Proctor and N.O. Weiss, Magnetoconvection. *Reports on Progress in Physics* 45 (1982) 1317–1379.
5. H.E. Huppert and R.S.J. Sparks, Double-diffusive convection due to crystallization in magmas. *Ann. Rev. Earth and Planetary Sci.* 12 (1984) 11–37.
6. J.S. Turner, Multicomponent convection. *Ann. Rev. Fluid Mech.* 17 (1985) 11–44.
7. S.M. Cox, S. Leibovich, I.M. Moroz and A. Tandon, Non-linear dynamics in Langmuir circulations with O(2) symmetry. *J. Fluid Mech.* 241 (1992) 669–704.
8. S.M. Cox, S. Leibovich, I.M. Moroz and A. Tandon, Hopf bifurcations in Langmuir circulations. *Physica* 59D (1992) 226–254.
9. I. Langmuir, Surface motion of water induced by wind. *Science* 87 (1938) 119–123.
10. S. Leibovich, The form and dynamics of Langmuir circulations. *Ann. Rev. Fluid Mech.* 15 (1983) 391–427.
11. S. Leibovich, S. Lele and I.M. Moroz, Non-linear dynamics in Langmuir circulations and in thermosolutal convection. *J. Fluid Mech.* 198 (1989) 471–511. Corrigendum in *J. Fluid Mech.* 235 (1992) 690.
12. J.M. Hewitt, D.P. McKenzie and N.O. Weiss, Large aspect ratio cells in two-dimensional thermal convection. *Earth and Planetary Sci. Lett.* 51 (1980) 370–380.

13. M.C. Depassier and E.A. Spiegel, The large-scale structure of compressible convection. *The Astron. J.* 86 (1981) 496–512.
14. D.T.J. Hurle, E. Jakeman and E.R. Pike, On the solution of the Bénard problem with boundaries of finite conductivity. *Proc. Roy. Soc. Lond.* A296 (1967) 469–475.
15. D.A. Nield, The thermohaline Rayleigh–Jeffreys problem. *J. Fluid Mech.* 29 (1967) 545–558.
16. E.M. Sparrow, R.J. Goldstein and V.K. Jonsson, Thermal instability in a horizontal fluid layer: effect of boundary conditions and non-linear temperature profile *J. Fluid Mech.* 18 (1964) 513–528.
17. C.J. Chapman and M.R.E. Proctor, Non-linear Rayleigh–Bénard convection between poorly conducting boundaries. *J. Fluid Mech.* 101 (1980) 759–782.
18. V.L. Gertsberg and G.I. Sivashinsky, Large cells in non-linear Rayleigh–Bénard convection. *Prog. Theor. Phys.* 66 (1981) 1219–1229.
19. M.R.E. Proctor, Planform selection by finite-amplitude thermal convection between poorly conducting slabs. *J. Fluid Mech.* 113 (1981) 469–485.
20. G.I. Sivashinsky, Large cells in non-linear Marangoni convection. *Physica* 4D (1982) 227–235.
21. S.M. Cox and S. Leibovich, Large-scale Langmuir circulation and double-diffusive convection: Evolution equations and flow transitions. Submitted (1993).
22. E. Knobloch, Pattern selection in long-wavelength convection. *Physica* 41D (1990) 450–479.
23. E. Knobloch, Doubly diffusive waves. In: N.E. Bixler and E. Spiegel (eds), *Double Diffusive Motions.* American Society of Mechanical Engineers, FED 24 (1985) 17–22.
24. F.H. Busse and N. Riahi, Non-linear convection in a layer with nearly insulating boundaries. *J. Fluid Mech.* 96 (1980) 243–256.
25. G.I. Sivashinsky, On cellular instability in the solidification of a dilute binary alloy. *Physica* 8D (1983) 243–248.
26. S.M. Cox and S. Leibovich, Langmuir circulations in surface layer bounded by a strong thermocline. *J. Phys. Oceanogr.* 23 (1993) 1330–1345.
27. M.C. Depassier and E.A. Spiegel, Convection with heat flux prescribed on the boundaries of the system. I. The effect of temperature dependence of material properties. *Geophys. Astrophys. Fluid Dynam.* 21 (1982) 167–188.
28. P. Cessi and W.R. Young, Multiple equilibria in two-dimensional thermohaline circulation. *J. Fluid Mech.* 241 (1992) 291–309.
29. P. Cessi, Metastability and transition between equilibria in β-plane thermohaline convection. Preprint (1993).
30. G. Dangelmayr and E. Knobloch, Interaction between standing and travelling waves and steady states in magnetoconvection. *Phys. Lett.* A 117 (1986) 394–398.
31. G. Dangelmayr and E. Knobloch, The Takens–Bogdanov bifurcation with $O(2)$-symmetry. *Phil. Trans. Roy. Soc. Lond.* A 322 (1987) 243–279.
32. W. Schöpf and W. Zimmermann, Results on wave patterns in binary fluid convection. *Phys. Rev.* A 41 (1990) 1145–1148.
33. E. Knobloch and D.R. Moore, Linear stability of experimental Soret convection. *Phys. Rev.* A 37 (1988) 860–870.
34. E. Knobloch, Pattern selection in binary-fluid convection at positive separation ratios. *Phys. Rev.* A 40 (1989) 1549–1559.
35. E. Knobloch, Non-linear binary fluid convection at positive separation ratios. In: H. Takayama (ed.), *Cooperative Dynamics in Complex Physical Systems.* Springer Series in Synergetics (1989) Vol. 43, pp. 337–338.